NASA/TM-20220017061

Influences of Varied Electrical Discharge Machining Operations on Surface Conditions of Several Nickel-Based Superalloys

Timothy P. Gabb, Christopher A. Kantzos, Timothy M. Smith, Richard B. Rogers, and Jack Telesman
Glenn Research Center, Cleveland, Ohio

David J. Brinkman, Timothy J. Ubienski, and Ralph J. Pawlik
HX5 Sierra, Cleveland, Ohio

January 2023

NASA STI Program . . . in Profile

Since its founding, NASA has been dedicated to the advancement of aeronautics and space science. The NASA Scientific and Technical Information (STI) Program plays a key part in helping NASA maintain this important role.

The NASA STI Program operates under the auspices of the Agency Chief Information Officer. It collects, organizes, provides for archiving, and disseminates NASA's STI. The NASA STI Program provides access to the NASA Technical Report Server—Registered (NTRS Reg) and NASA Technical Report Server—Public (NTRS) thus providing one of the largest collections of aeronautical and space science STI in the world. Results are published in both non-NASA channels and by NASA in the NASA STI Report Series, which includes the following report types:

- TECHNICAL PUBLICATION. Reports of completed research or a major significant phase of research that present the results of NASA programs and include extensive data or theoretical analysis. Includes compilations of significant scientific and technical data and information deemed to be of continuing reference value. NASA counter-part of peer-reviewed formal professional papers, but has less stringent limitations on manuscript length and extent of graphic presentations.

- TECHNICAL MEMORANDUM. Scientific and technical findings that are preliminary or of specialized interest, e.g., "quick-release" reports, working papers, and bibliographies that contain minimal annotation. Does not contain extensive analysis.

- CONTRACTOR REPORT. Scientific and technical findings by NASA-sponsored contractors and grantees.

- CONFERENCE PUBLICATION. Collected papers from scientific and technical conferences, symposia, seminars, or other meetings sponsored or co-sponsored by NASA.

- SPECIAL PUBLICATION. Scientific, technical, or historical information from NASA programs, projects, and missions, often concerned with subjects having substantial public interest.

- TECHNICAL TRANSLATION. English-language translations of foreign scientific and technical material pertinent to NASA's mission.

For more information about the NASA STI program, see the following:

- Access the NASA STI program home page at http://www.sti.nasa.gov

- E-mail your question to help@sti.nasa.gov

- Fax your question to the NASA STI Information Desk at 757-864-6500

- Telephone the NASA STI Information Desk at 757-864-9658

- Write to:
  NASA STI Program
  Mail Stop 148
  NASA Langley Research Center
  Hampton, VA 23681-2199

NASA/TM-20220017061

Influences of Varied Electrical Discharge Machining Operations on Surface Conditions of Several Nickel-Based Superalloys

Timothy P. Gabb, Christopher A. Kantzos, Timothy M. Smith, Richard B. Rogers, and Jack Telesman
Glenn Research Center, Cleveland, Ohio

David J. Brinkman, Timothy J. Ubienski, and Ralph J. Pawlik
HX5 Sierra, Cleveland, Ohio

National Aeronautics and
Space Administration

Glenn Research Center
Cleveland, Ohio 44135

January 2023

Acknowledgments

The authors gratefully acknowledge the support of the Advanced Air Transport Technology (AATT) Project Office of NASA's Aeronautics Research Mission Directorate (ARMD). We recognize the work of Joy Buehler of HX5 Sierra for careful metallographic preparation of all sectioned test materials in the metallography lab of the Analytical Sciences Group at NASA Glenn Research Center. The authors appreciate the work performed by Peter Bonacuse of the Analytical Science Group at NASA Glenn Research Center in facilitating our evaluations of roughness, residual stress, surface appearance, and microstructures via electron microscopy. Glen Bigelow has also earned our thanks for his thoughtful review of this manuscript.

This work was sponsored by the
Transformative Aeronautics Concepts Program.

Level of Review: This material has been technically reviewed by technical management.

This report is available in electronic form at https://www.sti.nasa.gov/ and https://ntrs.nasa.gov/

Influences of Varied Electrical Discharge Machining Operations on Surface Conditions of Several Nickel-Based Superalloys

Timothy P. Gabb, Christopher A. Kantzos, Timothy M. Smith, Richard B. Rogers, and Jack Telesman
National Aeronautics and Space Administration
Glenn Research Center
Cleveland, Ohio 44135

David J. Brinkman, Timothy J. Ubienski, and Ralph J. Pawlik
HX5 Sierra
Cleveland, Ohio 44135

Summary

Nickel-based superalloys designed for use in gas turbine engine blades are difficult and expensive to machine properly without producing undue surface damage, in part because of their superior mechanical properties at high temperatures. Numerically controlled electrical discharge machining (EDM) is now commonly used as a machining process for initial sectioning, detailed roughing, and even some finishing operations in these applications. The objective of this study was to examine the effects of EDM on the surface conditions of superalloy 718 after slicing using typical rough, semi-finish, and finish condition sets with a typical wire EDM machine. Surface roughness, residual stress, and microstructures were compared for these conditions. The varied EDM conditions influenced surface roughness as intended. The residual stresses and surface roughness directly corresponding to the EDM steps were determined. Although roughness decreased when progressing from rough to finish EDM conditions, tensile residual stresses unexpectedly increased. Brief assessments after EDM of two higher performance powder metallurgy disk superalloys, ME209 and LSHR, indicated this inverse relationship of roughness versus tensile residual stress was also present for these superalloys, where tensile residual stresses were significantly enhanced.

Introduction

Nickel-based superalloys designed for use in gas turbine engines as disks and blades can be difficult and expensive to machine, in part as a result of their superior mechanical properties at high temperatures (Ref. 1). Milling, turning, and grinding operations require high-performance tools and controls to machine superalloys without excessive geometric deviations, surface roughness, plastic damage, brittle layers, other microstructural disturbances, and residual stresses that impair their intended properties. Electrical discharge machining (EDM) can be used as an alternative machining process for roughing or initial sectioning operations through finishing operations.

Modern EDM processing has been reviewed in Reference 2. In the EDM process, an electrode is moved close enough to the workpiece to produce a sufficient small gap for a voltage to ionize a working fluid (dielectric) into plasma, which erodes both the electrode and the workpiece (Refs. 2 and 3). This "gap" voltage is generated using a current applied as pulses in cycles at high frequencies ranging from near 10 kHz to higher than 1 MHz. Between each "time on" current pulse, the intervening "time off" allows channeled dielectric fluid to flush away metal debris generated by the workpiece and by the electrode tool. The present study focuses on the use of a wire EDM process to section superalloys, in

which a wire negative electrode is continuously fed at a constant rate to section a positive electrode workpiece, and the dielectric flushes debris away from the narrow slot that is created.

The EDM process melts metal locally at the gap, resulting in varied roughness, damaged microstructure, and residual stresses at the surface of the workpiece. Machining operations are very often specified based on the considerations of surface roughness and melted (recast) layer thickness, so these aspects have been extensively studied in wire EDM sectioning of engineering alloys, including the very widely used cast and wrought superalloy 718. In this manuscript, Inconel 718® (Special Metals Corporation) and other superalloys with effectively the same composition will be referred to as "superalloy 718."

Surface roughness has been reported to increase with higher discharge energy (Refs. 3 and 4). This discharge energy is the product of the maximum voltage, current, and on time (Ref. 5). Evaluations have also been made of the extent of microstructural damage left on the sliced surface in the form of a "recast" or "white" layer of melted and resolidified metal, as well as an underlying heat-affected zone (Refs. 2 and 3). The presence and thickness of the EDM recast layer and heat-affected zone have also been related to discharge energy. Assessments and measurements of heat-affected zones are more difficult to generalize, but they often include observations of annealed microstructures and their associated microhardness values. In many instances, these trends have encouraged the use of multiple passes, in which a first cutting operation at "rough" conditions at high discharge energy is followed by "finishing" passes at lower discharge energy to result in relatively lower levels of roughness and damaged layers (Refs. 3, 4, and 6).

Residual stresses and associated damage at the surfaces sectioned with EDM are not typically specified for engineering applications, and very limited research on this topic has been published for superalloys. However, this response was screened for some wire EDM applications on turbine disks made of UDIMET® alloy 720 (Special Metals Corporation) (Ref. 7). Here, tensile residual stresses generated in wire EDM of this material and surface roughness were higher when using roughing EDM conditions than for finishing EDM conditions, with residual stresses for roughing conditions approaching 600 MPa. This was found to significantly impair the fatigue life of tested coupons.

Significant modifications of the wire EDM process have been developed over the past decade to further address some of the issues described. For example, "clean cut" generator technologies use increased current frequency with carefully tailored waveform profiles, potentially in multiple passes (Refs. 6 and 7). These processes have been applied with promising results for various turbine disk features, including slots for blades and other contoured features, often meeting dimension specifications with minimized roughness, damage, and residual stresses. Such wire EDM processes have the potential for use in screening prototype designs for cooling holes, bolt holes, fillets, blade slots, and other details. Therefore, EDM applications will likely continue to proliferate as these technologies and related sensing and computer control methods advance.

However, it is not clear if a developed specific set of process settings for a wire EDM process can be widely applied across different superalloys. Candidate superalloys for which EDM could be applied for turbine disk applications include widely used conventional cast and wrought superalloys, as well as higher performance powder metallurgy (PM) superalloys. Although post-EDM surface conditioning such as polishing and shot peening could eventually be planned after EDM processing for some applications, it would still be important to understand the state of as-machined surfaces for applying such subsequent conditioning treatments properly.

The primary objective of this study was to examine the resulting surface conditions of typical cast and wrought superalloy 718 after sectioning using typical roughing, semi-finishing, and finishing EDM condition sets with a typical EDM machine. Standard brass wire with a nominal composition of Cu-40Zn

in weight percent was used to machine several sections. Surface roughness, residual stresses, and microstructure were compared for the varied EDM condition sets. A secondary objective was to assess how these trends for roughness and residual stresses compare for two higher performance PM disk superalloys, ME209 (Ref. 8) and LSHR (Ref. 9). These results could later be supplemented with low-cycle fatigue testing to assess the influence of varied EDM techniques on this surface-sensitive mechanical property.

Materials and Procedure

Table I lists the composition in weight percent of superalloy 718, LSHR, and ME209. Superalloy 718 was obtained as a conventionally cast and wrought bar in the solution annealed state. It was tested in the solution annealed state because this particular alloy can often be machined in this state for its multitude of applications. LSHR was produced using PM processing, including hot isostatic pressing, extrusion, and isothermal forging (Ref. 10). A rectangular section was then solution heat treated at 1,171 °C for 2 h, then was aging heat treated at 855 °C for 4 h followed by 775 °C for 8 h. ME209 was produced using PM processing, including hot compaction, extrusion, isothermal forging, and a heat treatment similar to that used for the LSHR specimen (Ref. 8). Figure 1 shows typical microstructures of all three alloys. LSHR and ME209 were tested in the solution plus aging heat-treated state because these higher performance superalloys can more often be machined in this latter state for their more focused turbine disk applications.

Specimens of each alloy were sectioned using a Sodick AQ300L wire electrical discharge machine. Standard hard brass wire (HQ hard brass wire, Cu-40Zn nominal weight percent, Hightech Division of Sodick) at 0.25 mm in diameter was used as the electrode at a constant wire feed rate of 70 mm/min. Distilled water was used as the dielectric at a high-pressure flush setting for all runs. Conditions referred to as “rough,” “semi-finish,” and “finish” were used in single-pass slicing operations, using the standard terminology and condition sets described in the Sodick user manual (Ref. 11), summarized in Table II. The rough condition used the highest gap voltage, on time, off time, current, and specimen feed rate; the finish condition used the lowest gap voltage, on time, off time, and specimen feed rate, combined with medium current level; and the semi-finish condition also used low voltage, on time, off time, and specimen feed rate, but at medium current level. Alternating-current (AC) mode was used for rough condition sets; direct-current (DC) mode was used for semi-finish and finish condition sets. The condition sets were those recommended in the user manual for steels, which required only slight adjustments during slicing to maintain stable response for all the tested superalloys.

Roughness and residual stresses were measured in the x-direction perpendicular to the brass wire and the y-direction parallel to the wire, as defined in Figure 2. The roughness of the machined surfaces was measured with a Zygo Nexview™ NX2 white light interferometer at a magnification of ×5. The surfaces were also examined using a JEOL 6100 scanning electron microscope (SEM), where the composition of surface features could be determined using energy dispersive x-ray spectroscopy (EDS). Residual stresses and x-ray peak width were measured with a D8 DISCOVER® (Bruker) x-ray diffractometer equipped with a General Area Detector Diffraction System (GADDS) and using a Mn tube, then analyzed using the Bruker LEPTOS V.7 software. The angle of the K-alpha peak of the (311) plane was measured at different tilting positions to determine residual stresses. The width of the peak at half of maximum intensity was measured to signify damage at the surface. Instrument alignment was verified per ASTM E915, with procedures adapted to the area detector. In some cases, thin layers of surface material were electropolished away using a Proto model 8818-V2 portable electrolytic polisher before measuring residual stress and peak width again. Some of these machined superalloy specimens were also exposed at 704 °C for 24 h in vacuum to assess the relaxation of these stresses at the EDM surface.

Repeated cycles of electropolishing and x-ray analysis of surfaces were performed on specimens machined using each condition set. The depths of electropolishing were measured at each cycle using the white light interferometer. The effect of removing material on the subsequently measured stresses was then determined using the appropriate stress relationships (Ref. 12), allowing stresses to be corrected for this layer removal. This allowed generation of depth profiles of the biaxial residual stresses.

Metallographic cross sections of the EDM surfaces were mounted in PolyFast mounting material, then ground and polished using a Struers AbraPol-30 grinding and polishing machine. These specimens were examined in the unetched condition using a Hitachi 4700 field emission scanning electron microscope (FESEM) with an accelerating voltage of 20 kV to characterize selected areas in detail, at working distances of 10 to 20 mm. Secondary electron images were obtained using a Hitachi 4700 FESEM. Backscattered electron images were obtained using the SEM's backscatter electron detector. An Oxford Instruments X-Max 50 energy dispersive x-ray spectrometer (EDS), which was integrated into the FESEM, was used to create x-ray maps of the damaged areas at a working distance of about 12 mm. The spectrometer detects x rays that are characteristic of each element present at the point excited by the electron beam. These elemental x-ray maps of scanned areas allow the locations and compositions of the surface and any embedded materials to be estimated.

Results

Electrical Discharge Machined Surfaces of Superalloy 718

The surface appearance varied with EDM condition set for superalloy 718, as shown in the SEM images in Figure 3. The backscattered electron SEM images showed variations in brightness, suggesting local changes in topography, and potentially also in average atomic number and, therefore, composition. Energy dispersive x-ray analysis of the points identified in the images are given in Table III. Many points had significant levels of Cu and Zn, indicative of contamination from the melting brass wire. Such contamination has been reported in studies of various superalloys sectioned using EDM with brass wire (Ref. 3 and 4). High oxygen levels were also measured on these EDM surfaces. Similar degrees of this contamination were observed in the present study for all three condition sets.

Rough conditions gave the coarsest visual texture; semi-finish and finish condition sets produced finer visual texture. Figure 4 shows overall macroscopic roughness versus condition as measured using white light interferometry. Average roughness (R_a), root mean square roughness (rms), and peak-valley roughness (P-V) varied with the EDM condition sets. Rough conditions produced the highest R_a, rms, and P-V values. The corresponding roughness measurements for semi-finish and finish EDM condition sets were about 50 percent lower than those for rough conditions. In these plots, hollow symbols indicate measurements parallel to the wire; filled symbols indicate measurements perpendicular to the wire. One-way analyses of variance (ANOVA) indicated no significant differences were present between roughness measurements in the x- and y-directions for any of the three EDM condition sets. This agrees with the findings previously reported in another study using a different Sodick machine for wire EDM of superalloy 718 (Ref. 4).

The residual stresses of as-machined surfaces also varied between EDM condition sets, as shown in Figure 5. Semi-finish and finish condition sets that gave reduced roughness produced higher levels of tensile residual stresses. One-way analysis of variance indicated the semi-finish and finish condition sets produced significantly higher mean tensile residual stresses at the surface than those measured for the rough condition set. This was in contradiction to the trends for roughness, in which semi-finish and finish condition sets gave lower roughness than for the rough condition set. One-way ANOVA indicated no

significant difference in residual stress was measured between the x- and y-directions for any of the three EDM condition sets.

Depth Profiles for Electrical Discharge Machined Surfaces of Superalloy 718

Residual Stress

Repeated cycles of electropolishing plus x-ray analysis of surfaces were performed on specimens machined using each condition set to give depth profiles of the biaxial residual stresses. The biaxial residual stresses are shown versus depth in Figure 6(a). Substantial tensile residual stresses persisted to a depth of near 10 μm for the semi-finish and finish condition sets, and near 20 μm for the rough condition set. A second group of specimens machined using each condition set was later exposed to a high temperature of 704 °C for 24 h in vacuum, then analyzed in the same way as the first group. This was intended to screen the effects of service near the upper limit of application temperatures for superalloy 718. The biaxial residual stresses measured after exposure are shown versus depth in Figure 6(b). The exposure to high temperature relaxed but did not eliminate tensile stresses at and near the surface. As previously observed, no consistent variation in these responses was observed between the x- and y-directions.

Microstructure

Typical microstructures near the surface, including recast layers and heat-affected zones, were studied in cross sections for the varied EDM condition sets using optical and field emission scanning electron microscopy. Figure 7 and Figure 8 show typical microstructures prepared transverse to the EDM sliced surfaces. The optical and FESEM images in Figure 7 show the substantial decrease in surface roughness when the semi-finish and finish condition sets are substituted for the roughing condition set. Grain structure and phases can be discerned in the FESEM images. Backscattered scanning electron images show an interior microstructure having delta phase visible at most of the grain boundaries. However, the delta phase becomes absent when the surface is approached. An outer recast region with fine pores is evident, with scattered wire contaminant particles of high Cu and Zn embedded in it.

As illustrated in the annotated micrographs of Figure 8, the thicknesses of the recast layer and the heat-affected zone are not very consistent. Measured from the surface recast region, the depth of the recast layer was defined as the distance where the recast pores terminate, as delineated in Figure 8 with a green dashed line. The thickness of the recast layer varies considerably. For the rough condition set, large recast bumps extend out up to 40 μm; in adjacent locations, the recast layer is much narrower. This inconsistency could be due to the discontinuous formation of recast layers as well as recast particles during EDM slicing, with the particles and fragments separating from the surface. The semi-finish and finish condition sets have more modest recast bumps, extending out up to 8 μm. Yet, with all three condition sets, the recast layer thickness varied significantly. This agrees with the findings of others for various alloys sectioned using wire EDM (Refs. 3 and 4). The thickness of this layer was therefore defined in Table IV, with minimum, median, and maximum values, as well as mean and standard deviation, for each condition set. The mean values were compared using one-way ANOVA. The mean recast layer thickness produced by the semi-finish condition set was found to be higher than that produced using the rough and finish condition sets. This is in general agreement with other studies on wire EDM of superalloys (Refs. 4 and 5). Composition measurements in these recast layers did not differ substantially from the bulk, with the exception of Cu, Zn (arrows) and the higher O often observed. This trend is generally consistent with several other studies of EDM of superalloys, including superalloy 718 (Refs. 4 and 5).

The heat-affected zone was defined here as beginning at the green dashed line where the recast pores terminated and ending where the delta phase of the interior microstructure reappeared. This is indicated with a yellow dashed line in Figure 8. The heat-affected zone thickness also varied widely. Minimum, median, and maximum measured heat-affected zone thicknesses are included in Table IV along with the mean and standard deviations. The semi-finish condition set gave the highest median thickness of the heat-affected zone, with the finish condition set giving a slightly lower thickness. The rough condition set produced the lowest thickness. This result was unexpected, not being reported in References 4 and 5. Analysis by one-way ANOVA confirmed this ranking. However, the low coefficient of determination ($R^2 = 0.33$) reflected the variability in these measurements and limited the ability to compare these values.

Electrical Discharge Machined Surfaces and Stress Profiles of Two Higher Strength Powder Metallurgy Superalloys

The same EDM condition sets were applied for sectioning two higher strength PM disk superalloys, ME209 and LSHR, and the surface appearance varied with EDM condition set as it did for superalloy 718, shown in the SEM backscattered electron images of Figure 9. Energy dispersive x-ray analysis again indicated spots having significant levels of Cu and Zn, indicative of contamination from the melting brass wire. Comparable degrees of this contamination were observed for all three condition sets for all three superalloys.

Comparable trends of roughness were also apparent with varied EDM condition sets for the two PM disk superalloys. Just as with superalloy 718, roughing conditions gave the coarsest visual texture; semi-finishing and finishing conditions produced finer visual texture. Overall macroscopic roughness as measured using white light interferometry is shown versus condition and alloy in Figure 10. Measurements were again made for ME209 and LSHR specimens in the x- and y-directions. Average roughness (R_a) and peak-valley roughness (P-V) measurements, made in the y- (wire) direction, are shown in Figure 10 for varied EDM condition sets. Rough conditions also produced the highest R_a and P-V values for the PM superalloys. The corresponding roughness measurements for semi-finish and finish EDM conditions were about 50 percent lower than those for rough conditions. The roughness values measured for the PM superalloys were similar to those measured for superalloy 718; however, further comparisons were warranted.

One-way analyses of variance indicated no significant differences between measurements in the x- and y-directions for each of the alloys. This allowed combining the values measured in each direction to compare mean roughness values between the different alloys. The latter comparisons by one-way analyses of variance indicated that after using the rough condition set, ME209 had the highest mean P-V roughness at a confidence of greater than 95 percent, with 718 and LSHR having slightly lower values. For semi-finish and finish conditions, superalloy 718, ME209, and LSHR all had lower mean P-V roughness values that did not significantly vary between the alloys or these two condition sets. After using the rough condition set, ME209 had significantly higher mean R_a than 718 at a confidence of 95 percent; LSHR had an intermediate value. After using the semi-finish and finish condition sets, superalloy 718, ME209, and LSHR all had lower mean R_a values that did not vary significantly between the alloys or between these two condition sets.

The residual stresses of as-machined surfaces also varied between condition sets for the PM superalloys, as shown in Figure 11. Semi-finish and finish condition sets that resulted in reduced roughness generated approximately double the tensile residual stresses at the surface as those measured for the rough condition set. Although this trend was consistent with that observed for superalloy 718, the tensile residual stresses appeared to be higher for the PM superalloys. For residual stress, one-way analyses of variance again indicated no significant differences were present between measurements in the

x- and y-directions for each of the alloys. This allowed the values measured in each direction to be combined so that mean residual stress values between the different alloys could be compared.

Using the rough condition set on each alloy, LSHR had significantly higher mean tensile residual stress than superalloy 718 at a confidence of 95 percent; ME209 had an intermediate value. When using the semi-finish condition set, LSHR had significantly higher tensile residual stress than for all other combinations of alloy and EDM condition set. LSHR using the finish condition set had significantly higher average tensile residual stress than superalloy 718; ME209 had intermediate values.

For the PM superalloy specimens that had been machined using each condition set, repeated cycles of electropolishing plus x-ray analysis of surfaces were again performed in order to generate depth profiles of the residual stresses. The resulting residual stresses are shown versus depth in Figure 12(a). As observed for superalloy 718, substantial tensile residual stresses persisted to a depth of near 10 μm for the semi-finish and finish condition sets, and near 20 μm for the rough condition set. A second group of PM superalloy specimens machined using each condition set was then exposed to a high temperature of 704 °C for 24 h in vacuum before generating depth profiles of residual stress in the same way. This was intended to screen the effects of service near their upper limit of application temperatures. The residual stresses measured after exposure are shown versus depth in Figure 12(b). The exposure at high temperature relaxed, but did not eliminate, tensile stresses at and near the surface of the PM superalloys. The relaxed residual tensile stresses near and at the surface were significantly higher for the PM superalloys than those observed for superalloy 718. As previously observed for 718, no consistent variation in these responses was observed between the x- and y-directions for the ME209 or LSHR.

Discussion

The observed variations in roughness measured for these three superalloys have been observed in other studies of 718 and other superalloys (Refs. 4 and 5) and are consistent with the expectations of the EDM system manufacturer (Ref. 11). The contamination from the brass wire was also reported in many references (Refs. 1, 4, and 5). Rough conditions were identified in some of these studies as producing more contamination than for semi-finishing and finishing conditions. This could be due in part to the fact that semi-finishing and finishing condition sets were often applied there as finishing passes on surfaces that had already been sectioned (Ref. 4). It could be that fewer melted brass particles are entrapped in this surface “grazing,” compared to the present study with specimen sectioning using semi-finish and finish condition sets. Finishing passes on the open free surface would allow material to flow away instead of being constrained in a narrow slot/kerf, allowing more effective flushing.

The tensile residual stresses measured in this study were surprisingly high. Literature on EDM-processed surface residual stresses is limited. They were monitored in a study of UDIMET 720 alloy (Ref. 7), where values measured at the surface were comparable in magnitude to those observed here. No references could be located reporting the residual stresses generated by EDM of high-strength PM disk superalloys.

The lack of significant differences in both roughness or residual stress profiles between semi-finish and finish condition sets for all three superalloys deserves further consideration. Comparisons of these two corresponding EDM condition sets in Table II indicate two variables were unchanged: DC current mode and low specimen feed rate. It must be acknowledged that too many variables (six) changed in too few condition sets (three) to allow for rigorous linear regression to determine all influences of all six variables. However, it can be surmised that the current mode and specimen feed rate were very influential on both roughness and residual stress. The sustained DC current and low specimen feed rate correlated with low roughness, possibly related to a more uniform depth of spark erosion and melting than for the rough condition set. However, the sustained DC current and low specimen feed rate could be promoting a

greater depth of conduction heating, with subsequent contraction during cooling to promote tensile residual stresses near the surface, than for the rough condition set. This would also account for the greater depth of heat-affected zones for the semi-finish and finish condition sets in comparison to the rough condition set. The variations in voltage, on time, off (flush) time, and current level between the semi-finish and finish condition sets clearly had less influence on their responses of roughness and residual stress, although they may have modestly influenced the depth of the heat-affected zone.

Figure 13 illustrates a general scenario that could help explain the generation and persistence of the tensile residual stresses observed in this study. The high-pressure flushing by distilled water occurring during the EDM sectioning in this study can be considered a high-pressure water quench of the melted superalloy and the adjoining heated metal. This rapidly cooled contraction near the EDM surface is resisted by deeper, more slowly cooled material, generating tensile residual stresses near the surface. Precipitation-strengthened superalloys such as these are known to have higher strength and creep resistance when quenched at higher cooling rates (Ref. 13), even when not yet given aging heat treatments. In LSHR, this was associated with precipitation during the quench from the solution heat treatment of hyperfine tertiary γ' precipitates, which had to be resolved using transmission electron microscopy (Ref. 14). Therefore, this material adjacent to the EDM surface would be more resistant than the interior material to relaxation of stresses. These effects could be enhanced for PM superalloys with superior strength and creep resistance at high temperatures, in comparison to cast and wrought superalloy 718. This could help explain the higher tensile residual stresses measured on specimens as machined and after subsequent exposure at high temperatures for the PM superalloys.

Future Work

Fatigue testing is being considered to assess the influence of these varied EDM surfaces on this surface-sensitive mechanical property. Additional trials are planned to assess these responses after one or more finish passes are applied to sections previously sliced using the rough condition set. Other superalloys of varied microstructures, composition, strength, and creep resistance are also being considered for these evaluations.

Conclusions

The surface conditions of typical cast and wrought superalloy 718 (Inconel 718®, Special Materials Corporation) were evaluated after sectioning using electrical discharge machining (EDM) with typical rough, semi-finish, and finish condition sets on a typical wire EDM machine. Surface roughness, residual stresses, and microstructure were compared for the varied EDM condition sets. Roughness and residual stresses were then compared for two higher performance powder metallurgy (PM) disk superalloys, ME209 and LSHR. Several conclusions can be drawn from this work:

1. Surface roughness: Peak-valley and average surface roughness values are consistently reduced for semi-finish and finish EDM condition sets when compared with the rough condition set for all three sectioned superalloys.
2. Residual stresses: All three EDM condition sets resulted in tensile stresses present on the surface. The semi-finish and finish condition sets that reduce roughness generated approximately twice the tensile residual stresses of the rough condition set.
3. Microstructure: A recast layer of variable thickness can be produced by wire EDM in sectioning superalloy 718, especially for the rough condition set; however, the thickness of the underlying heat-affected zone thickness may not vary with the EDM condition set in the same order.

4. Higher performance PM superalloys: In comparison to cast and wrought superalloy 718, roughness variations with EDM condition sets can be very similar for higher performance PM superalloys, although the generated tensile residual stresses can be higher and more persistent because of these PM superalloys' greater resistance to stress relaxation.
5. Condition set variables: Among the settings varied for the three applied condition sets, it appears that current mode and specimen feed rate can influence roughness and residual stress during sectioning more strongly than the other four variables of voltage level, on time, off (flush) time, and current level.

References

1. Kappmeyer, G.; Hubiga, C.; Hardy, M.; Witty, M.; and Busch, M.: Modern Machining of Advanced Aerospace Alloys—Enabler for Quality and Performance. Procedia CIRP, vol. 1, 2012, pp. 28–43.
2. Pandey, Anand; and Singh, Shankar: Current Research Trends in Variants of Electrical Discharge Machining: A Review. Eng. Sci. Technol. An Int. J., vol. 2, no. 6, 2010, pp. 2172–2191.
3. Kern, Roger: Wire EDM Surface Characteristics and Their Evaluation. EDM Today, Summer 2018, pp. 10–15.
4. Li, L.; Guo, Y.B.; Wei, X.T.; and Li, W.: Surface Integrity Characteristics in Wire-EDM of Inconel 718 at Different Discharge Energy. Procedia CIRP, vol. 6, 2013, pp. 220–225.
5. Gostimirovic, Marin; Kovac, Pavel; Sekulic, Milenko; and Skoric, Branko: Influence of Discharge Energy on Machining Characteristics in EDM. J. Mech. Sci. Technol., vol. 26, no. 1, 2012, pp. 173–179.
6. Klocke, F.; Welling, D.; Klink, A.; Veselovac, D.; Nöthe, T.; and Perez, R.: Evaluation of Advanced Wire-EDM Capabilities for the Manufacture of Fir Tree Slots in Inconel 718. Procedia CIRP, vol. 14, 2014, pp. 430–435.
7. Antar, M.T.; Soo, S.L.; Aspinwall, D.K.; Sage, C.; Cuttell, M.; Perez, R., and Winn, A.J.: Fatigue Response of Udimet 720 Following Minimum Damage Wire Electrical Discharge Machining. Mater. Des., vol. 42, 2012, pp. 295–300.
8. Huron, E.S.; Bain, K.R.; Mourer, D.P.; and Gabb, T.: Development of High Temperature Capability P/M Disk Superalloys. Superalloys 2008, TMS, Warrendale, PA, 2008, pp. 181–190.
9. Gayda, J.; Gabb, T.P.; and Kantzos, P.T.: The Effect of Dual Microstructure Heat Treatment on an Advanced Nickel-Base Disk Alloy. Superalloys 2004, TMS, Warrendale, PA, 2004, pp. 323–330.
10. Gabb, T.; MacKay, R.A.; Draper, S.L.; Sudbrack, C.K.; and Nathal, M.V.: The Mechanical Properties of Candidate Superalloys for a Hybrid Turbine Disk. NASA/TM—2013-217901, 2013. https://ntrs.nasa.gov
11. Sodick Inc.: Wire EDM Machine Operation Training. Mark 25 Control, Part No. 6300009, 1999.
12. Moore, M.; and Evans, W.: Mathematical Correction for Stress in Removed Layers in X-Ray Diffraction Residual Stress Analysis. SAE Technical Paper 580035, SAE Trans., vol. 66, 1958, pp. 340–344.
13. Groh, J.: Effect of Cooling Rate From Solution Heat Treatment on Waspaloy Microstructure and Properties. Superalloys 1996, TMS, Warrendale, PA, 1996, pp. 621–626.
14. Gabb, T., Gayda, J.; Telesman, J.; and Garg, A.: The Effects of Heat Treatment and Microstructure Variations on Disk Superalloy Properties at High Temperature. Superalloys 2008, TMS, Warrendale, PA, 2008, pp. 121–130.

TABLE I.—COMPOSITION IN WEIGHT PERCENT OF TESTED MATERIALS

Alloy, wt.%	Al	B	C	Co	Cr	Fe	Mn	Mo	Ni	Nb	Si	Ta	Ti	V	W	Zr	Other
718	0.51	0.003	0.038	0.27	18.43	Bal.	0.12	3.06	52.5	5.16	0.045	0.005	0.86	-------	-----	-------	------
ME209	3.380	0.025	0.053	20.7	12.8	----	----	3.79	Bal.	0.9	-------	2.33	3.67	-------	2.03	0.049	------
LSHR	3.540	0.027	0.045	20.4	12.3	0.1	0.0	2.71	Bal.	1.49	0.012	1.52	3.45	0.0055	4.28	2.049	------

TABLE II.—CONDITIONS THAT WERE VARIED
DURING ELECTRICAL DISCHARGE MACHINING

EDM condition sets	Rough	Semi-finish	Finish
Voltage	High	Medium	Low
On time	High	Medium	Low
Off (flush) time	High	High	Low
Current	High	Low	Medium
Current mode	AC	DC	DC
Specimen feed rate	High	Low	Low

TABLE III.—ENERGY DISPERSIVE X-RAY ANALYSES OF COMPOSITION IN WEIGHT PERCENT
MEASURED AT SURFACE POINTS INDICATED IN FIGURE 3 FOR EDM 718

EDM condition set	Point	Al	Co	Cr	Fe	Mo	Ni	Nb	O	Ta	Ti	W	Cu	Zn
Rough	1	1.00	0.12	15.29	17.03	3.32	43.32	2.67	7.99	0.20	0.86	1.52	3.96	2.72
	2	0.34	0.25	18.55	15.57	2.53	36.31	3.37	7.23	1.19	1.21	1.07	7.53	4.85
	3	0.64	0.10	16.39	15.40	3.51	38.27	3.67	7.55	1.11	0.71	0.88	9.43	2.34
Semi-finish	1	3.76	0.20	8.62	9.87	2.73	22.52	1.44	31.04	1.05	0.48	0.72	5.37	12.21
	2	3.98	0.29	9.55	10.17	3.93	25.13	3.40	28.64	0.76	1.01	1.05	3.78	8.33
	3	3.09	0.60	12.08	14.21	2.62	35.51	1.22	16.76	0.05	0.64	1.37	3.97	7.89
Finish	1	4.93	0.25	8.78	9.78	2.48	23.82	1.43	32.65	-----	0.68	1.58	3.89	9.74
	2	5.60	0.16	9.53	9.46	2.40	24.29	1.97	30.65	-----	1.06	1.58	2.87	10.43
	3	4.09	0.06	10.33	10.69	2.89	25.46	2.77	27.13	-----	0.91	1.15	4.12	10.40

TABLE IV.—MEASURED THICKNESSES OF RECAST LAYER AND HEAT-AFFECTED ZONE INDICATED IN FIGURE 8 FOR ROUGH, SEMI-FINISH, AND FINISH EDM CONDITION SETS APPLIED TO SUPERALLOY 718

EDM condition sets		Rough	Semi-finish	Finish
Recast layer	Minimum, μm	0.8	1.5	1.4
	Maximum, μm	23.7	7.2	7
	Median, μm	11.3	4.6	3.1
	Mean, μm	11.8	4.9	3.4
	Standard deviation, μm	5.7	1.4	1.5
	Count	56	56	56
Heat-affected zone	Minimum, μm	1.4	1.7	1.4
	Maximum, μm	4.5	6.3	5.6
	Median, μm	2.7	3.2	2.7
	Mean, μm	2.7	3.4	2.8
	Standard deviation, μm	0.7	1.3	1
	Count	56	56	56

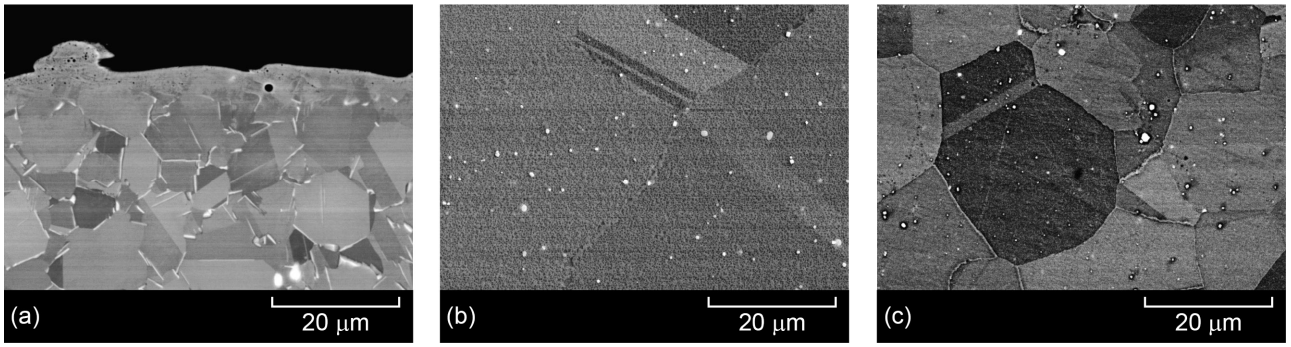

Figure 1.—Typical microstructures of tested alloys. (a) Superalloy 718. (b) ME209. (c) LSHR.

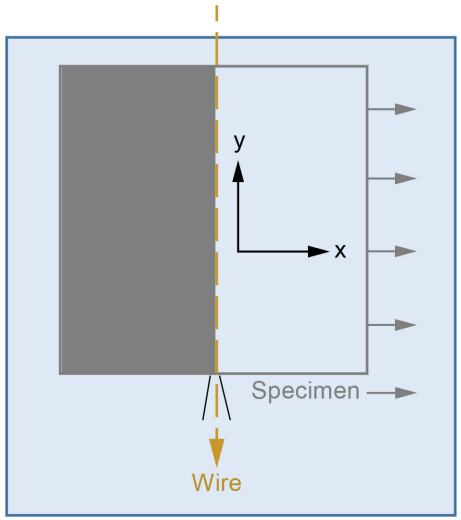

Figure 2.—Coordinate system used for roughness and residual stress measurements.

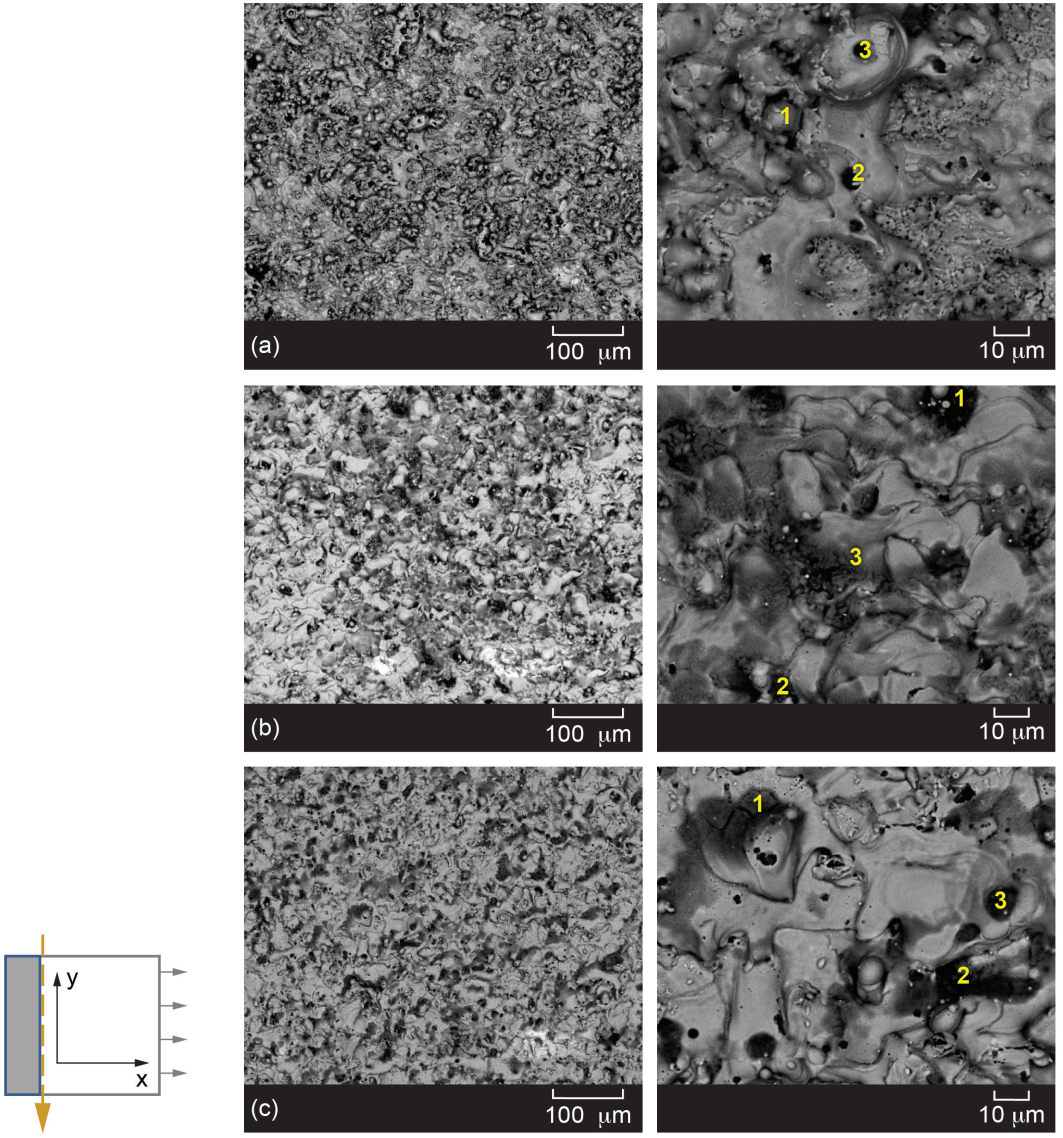

Figure 3.—Backscattered scanning electron images of superalloy 718 surfaces after EDM using different condition sets. Numbers indicate locations subjected to energy dispersive x-ray analysis (Table III). (a) Rough. (b) Semi-finish. (c) Finish.

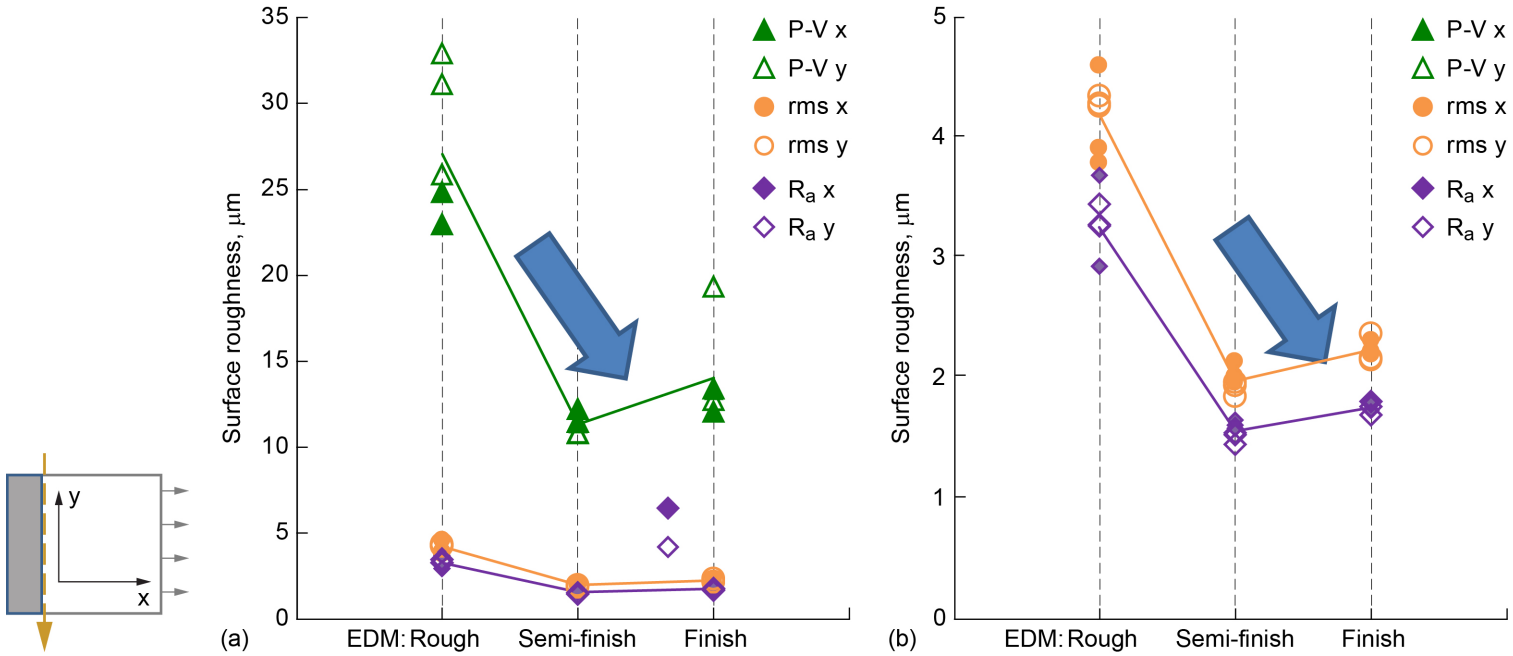

Figure 4.—Decreasing roughness of superalloy 718 surfaces after EDM for the rough, semi-finish, and finish condition sets.

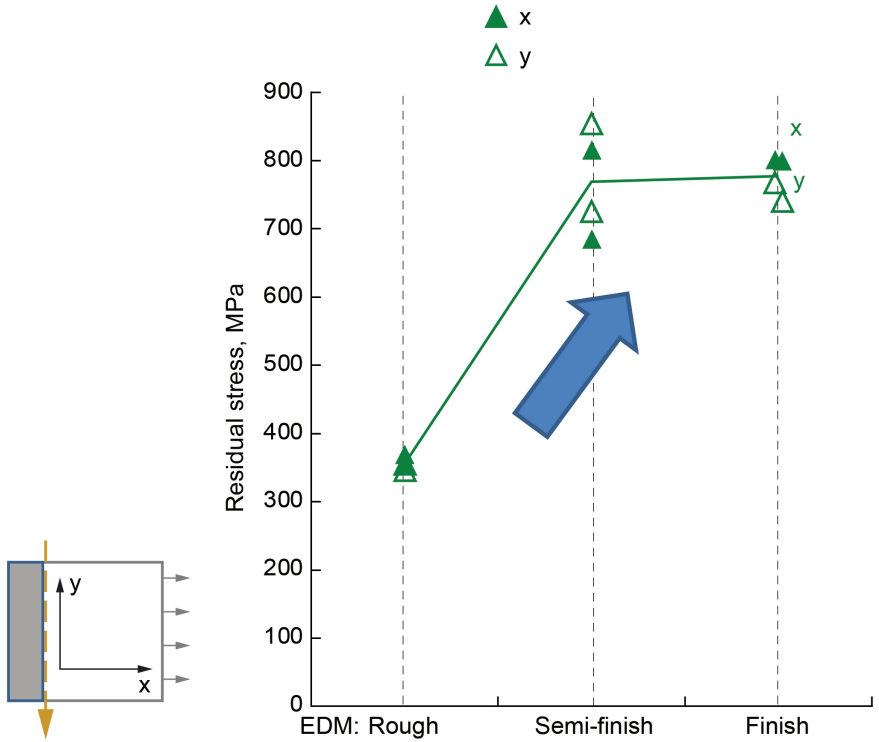

Figure 5.—Increasing residual stress at superalloy 718 surfaces after EDM for rough, semi-finish, and finish condition sets.

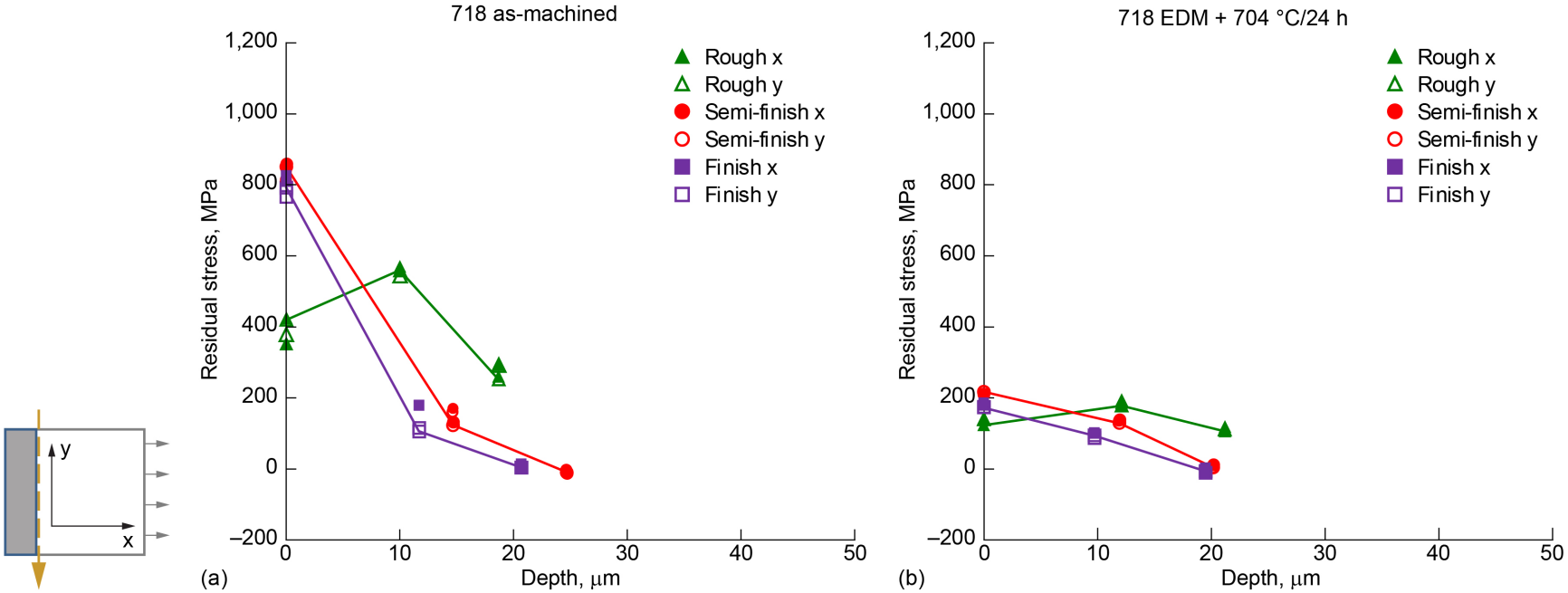

Figure 6.—Residual stress versus depth from the surface of superalloy 718 after EDM using rough, semi-finish, and finish condition sets. (a) As-machined. (b) Heated at 704 °C for 24 h in vacuum.

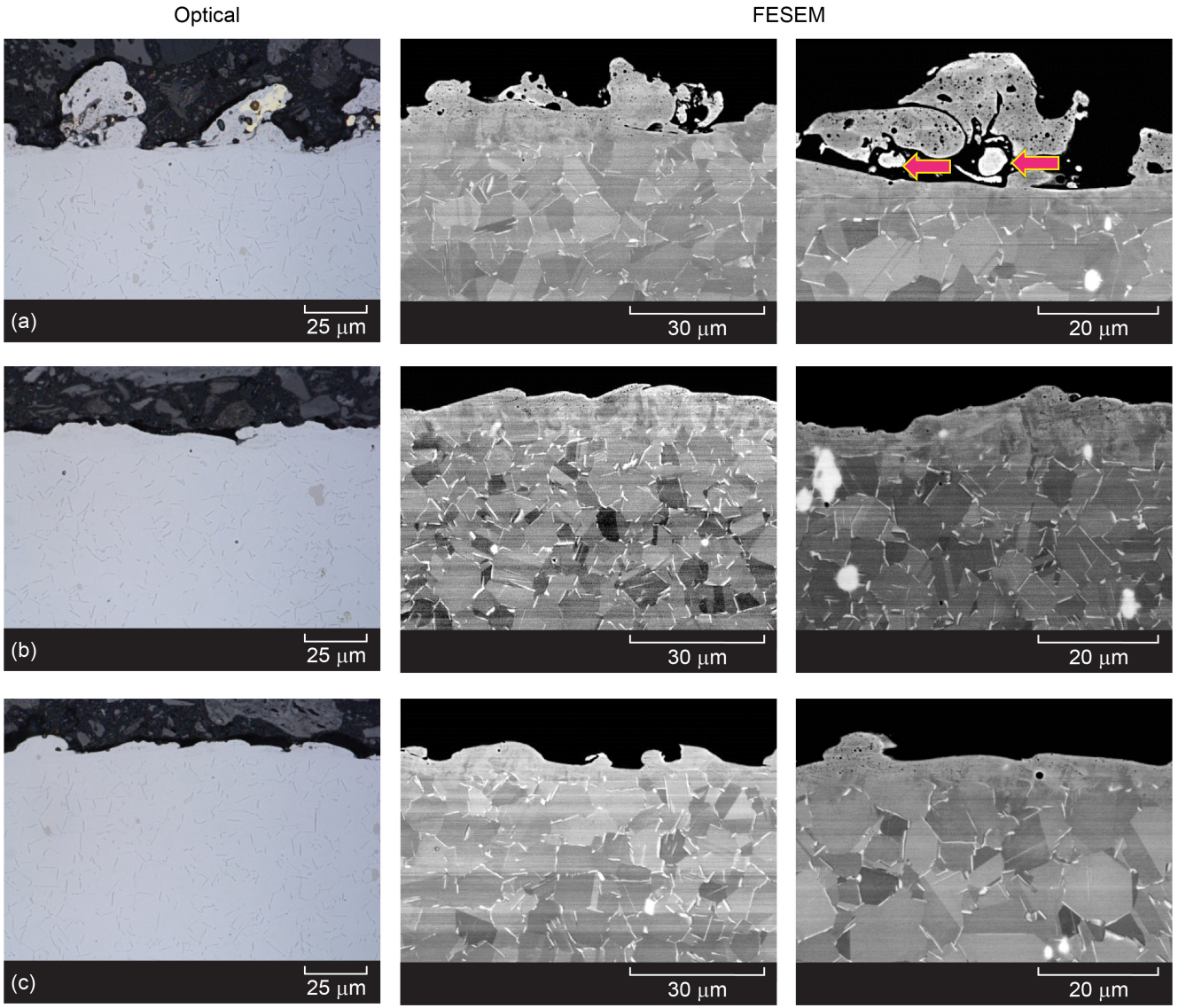

Figure 7.—Optical and field emission scanning electron microscope (FESEM) images of superalloy 718 versus depth from the surface after EDM using different condition sets. Arrows indicate brass wire contaminant particles containing high levels of Cu and Zn. (a) Rough. (b) Semi-finish. (c) Finish.

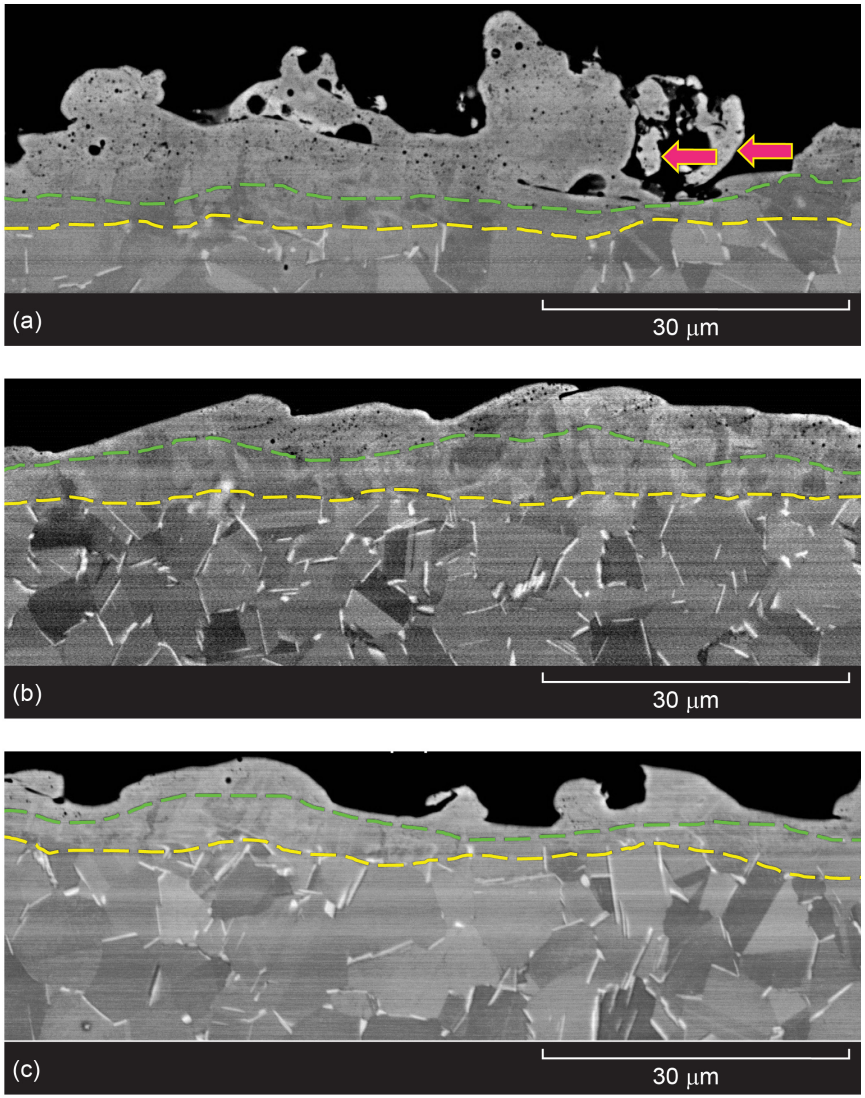

Figure 8.—Microstructures of superalloy 718 versus depth from the surface after EDM using different condition sets. (a) Rough. (b) Semi-finish. (c) Finish.

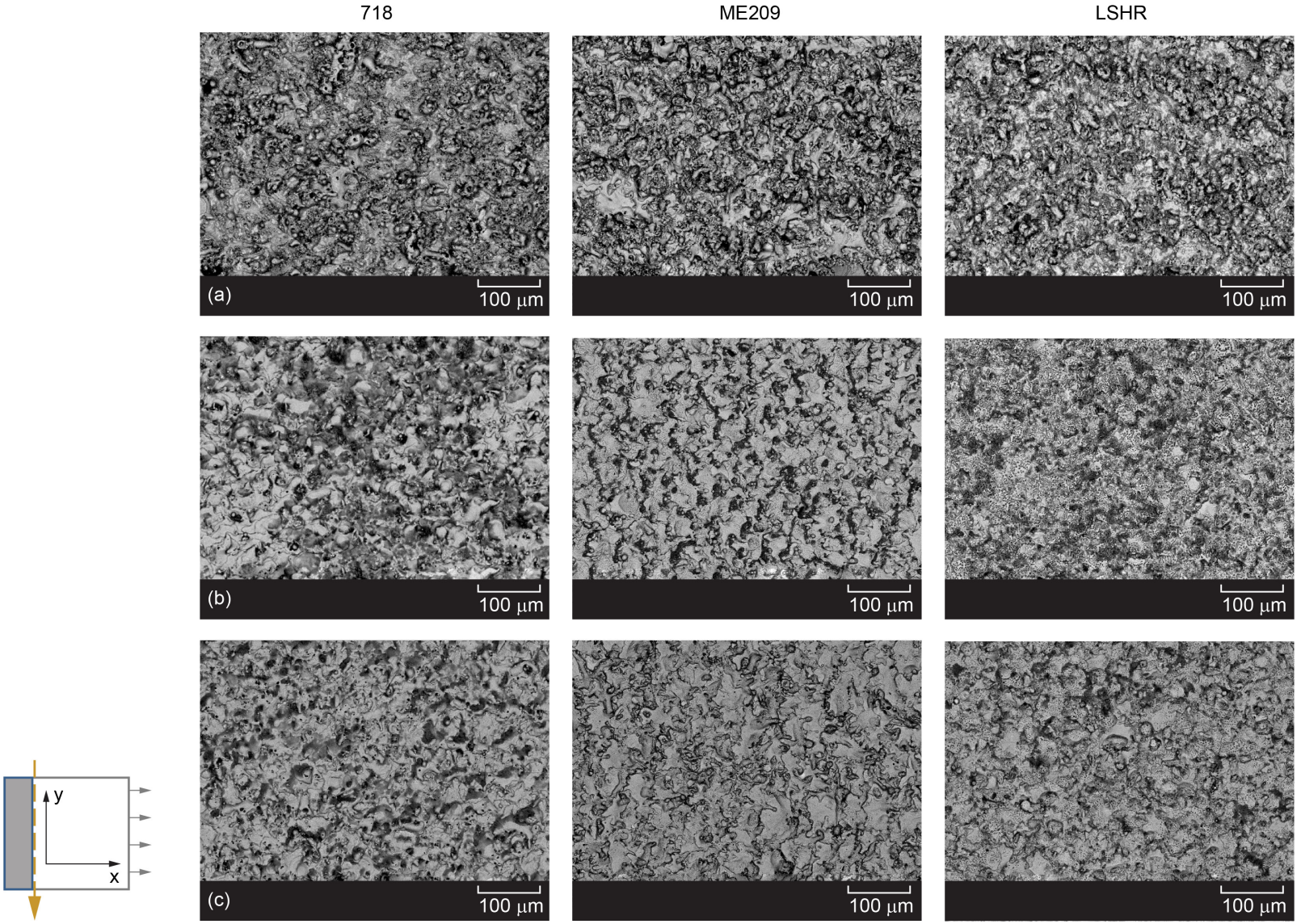

Figure 9.—Comparison of backscattered scanning electron images of superalloy surfaces after EDM sectioning using varied condition sets. (a) Rough. (b) Semi-finish. (c) Finish.

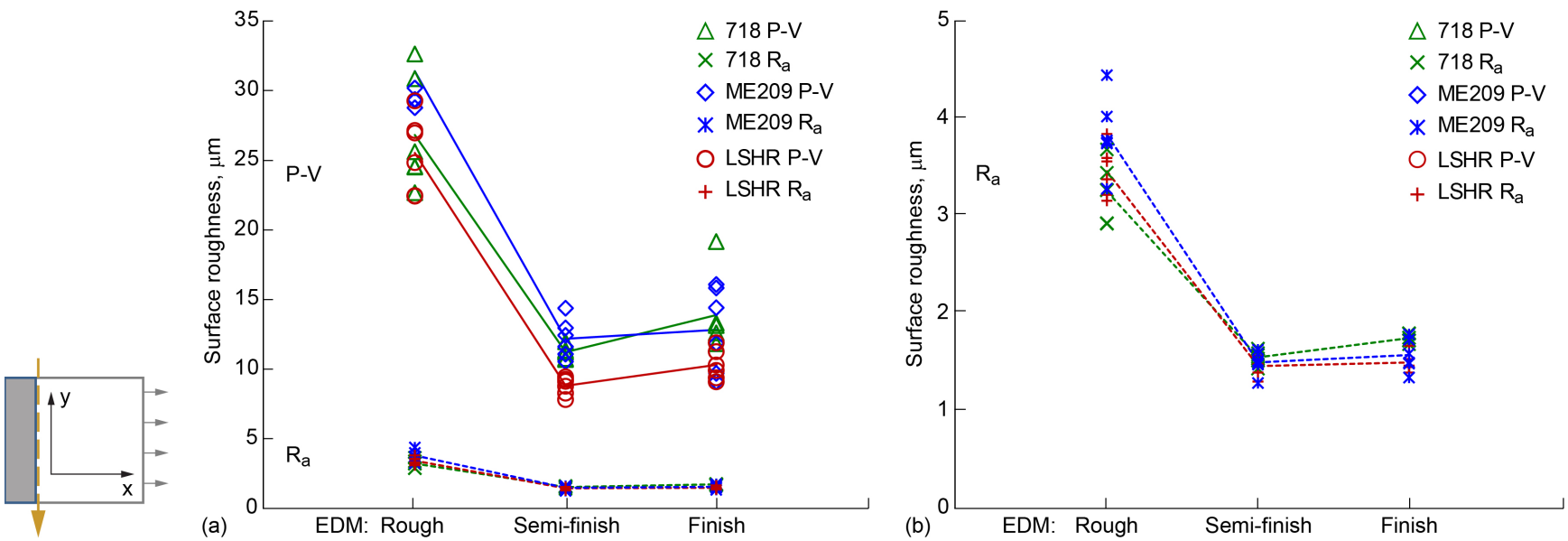

Figure 10.—Comparison of roughness in the y- (wire) direction for superalloy 718, ME209, and LSHR surfaces after EDM using rough, semi-finish, and finish condition sets.

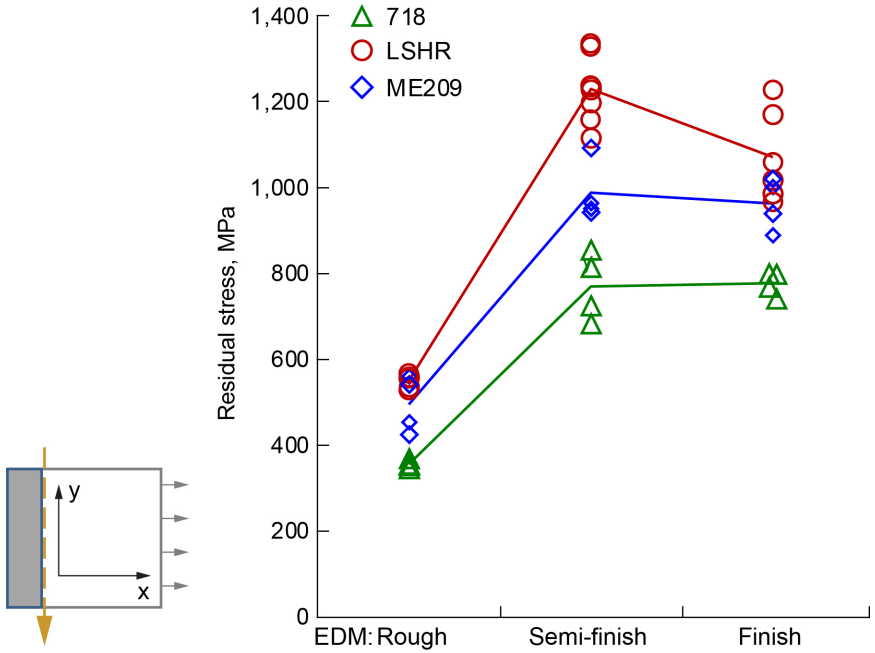

Figure 11.—Comparison of residual stress measured at the surface for superalloy 718, ME209, and LSHR after EDM using rough, semi-finish, and finish condition sets.

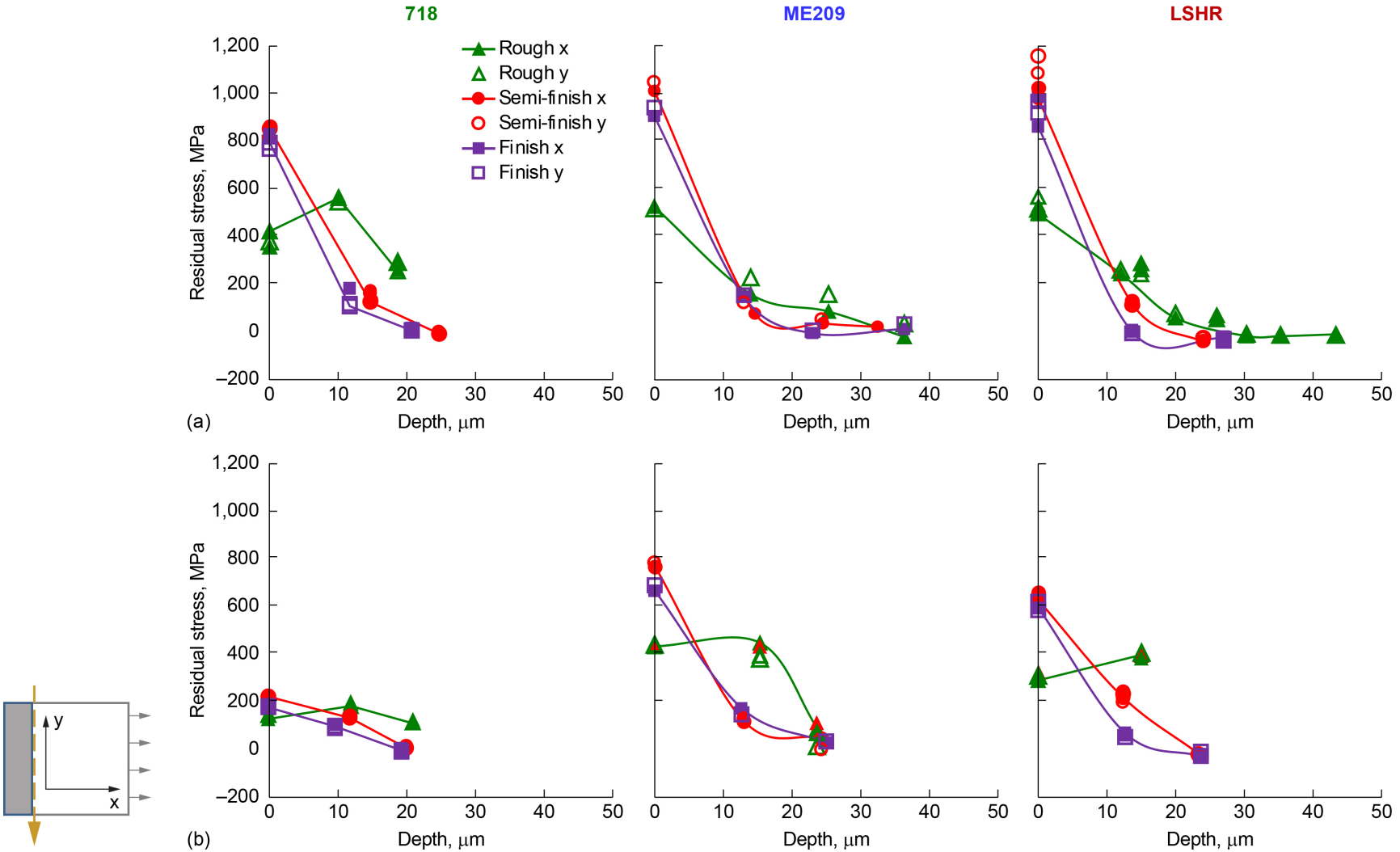

Figure 12.—Comparison of residual stress versus depth from the surface for superalloy 718, ME209, and LSHR after EDM using rough, semi-finish, and finish condition sets: (a) As-machined. (b) EDM plus heated at 704 °C for 24 h in vacuum.

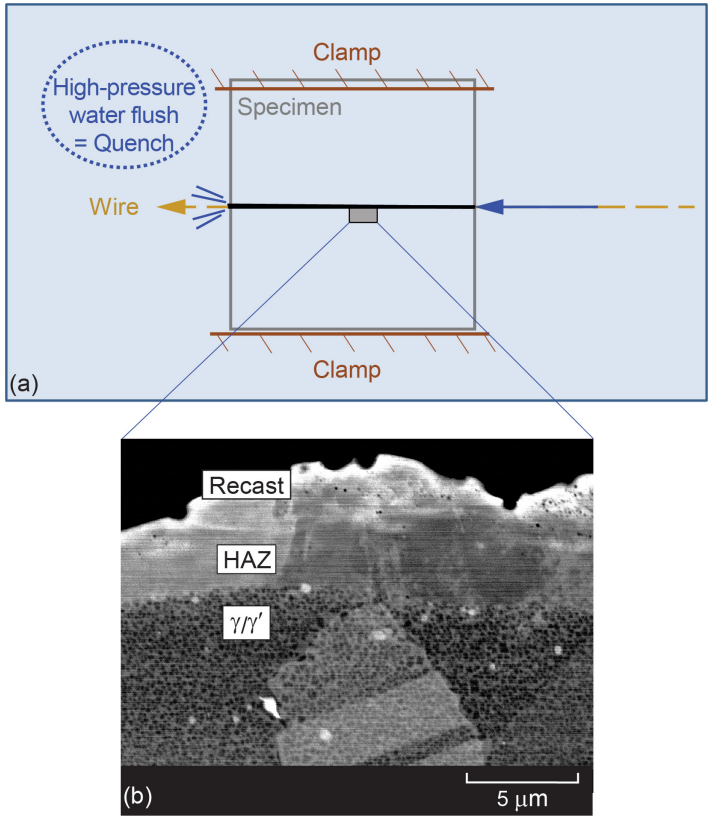

Figure 13.—(a) High-pressure water quenching during EDM sectioning of specimen. (b) FESEM image of LSHR cross section EDM using finish condition set, showing recast layer, heat-affected zone (HAZ), and γ′ precipitates in adjacent microstructure.